NASA TECHNICAL NOTE

NASA TN D-2197

FREE-FLIGHT INVESTIGATION OF MASS-TRANSFER COOLING ON A BLUNT CONE TO A MACH NUMBER OF 10.6

by Thomas E. Walton, Jr.

Langley Research Center
Langley Station, Hampton, Va.

NATIONAL AERONAUTICS AND SPACE ADMINISTRATION • WASHINGTON, D. C. • APRIL 1964

FREE-FLIGHT INVESTIGATION OF MASS-TRANSFER COOLING ON

A BLUNT CONE TO A MACH NUMBER OF 10.6

By Thomas E. Walton, Jr.

Langley Research Center
Langley Station, Hampton, Va.

FREE-FLIGHT INVESTIGATION OF MASS-TRANSFER COOLING ON

A BLUNT CONE TO A MACH NUMBER OF 10.6

By Thomas E. Walton, Jr.

SUMMARY

Mass-transfer cooling parameters are presented with large injection rates of nitrogen coolant in a laminar boundary layer for both a porous stagnation point and a nonporous conical afterbody of a blunted cone in free flight to a maximum Mach number of 10.6. A reasonable correlation of both the present porous stagnation results for large rates of mass injection and three-dimensional laminar stagnation theory for low and moderate rates of mass injection was obtained. A substantial reduction of the equilibrium wall temperature was achieved on the nonporous conical afterbody with mass injection at the stagnation point. There was no effect on the correlation of data due to Mach number and Reynolds number variation with time. The derivation of the effective heats of ablation from the present transpiration results provides an extension of theory to supercircular velocities.

INTRODUCTION

One of the many problems associated with the reentry of high-speed missiles and spacecraft is the problem of aerodynamic heating. A method currently under study at the Langley Research Center for alleviating this problem is the technique of mass-transfer cooling which includes both transpiration cooling and downstream cooling from upstream mass injection also referred to as film cooling.

Some exploratory investigations made with the objective of determining the potential of mass-transfer cooling were reported in references 1 and 2. Encouraging results from these ground facility experiments led to the initiation of a flight program to obtain results under free-flight conditions at supersonic speeds. Results of the initial flight investigation were reported in reference 3 which presented data to a Mach number of 4.08 on the effectiveness of transpiration cooling in a three-dimensional turbulent boundary layer on a relatively sharp 25° cone.

In the present investigation, interest is focused on blunt bodies, because the use of blunt leading edges and nose shapes is generally required for flight through the atmosphere at hypersonic speeds. This investigation was undertaken to study the effectiveness of reducing the convective heat transfer to both a

stagnation region and a conical afterbody of a blunted cone in hypersonic flight by incorporating both cooling schemes into a single system. The particular configuration considered was a 6° cone with a blunt porous nose cap. The technique was to inject nitrogen coolant through the porous nose cap and allow it to flow tangentially back over the conical afterbody and thereby cool the stagnation region by transpiration and the conical afterbody by film cooling.

In addition to the correlations of mass-transfer parameters presented herein, this paper also presents ablation parameters for laminar flow derived from the present transpiration results which are applicable to supercircular velocities.

The flight test was conducted at the NASA Wallops Station to a maximum Mach number of 13.7 by utilizing a four-stage vehicle. Because of telemetry failure, measured data ended during the burning of the fourth-stage motor; consequently, the useful data period extends to a maximum Mach number of 10.6 and over a Reynolds number per foot range from 1.36×10^6 to 3.76×10^6.

SYMBOLS

c	specific heat of skin material, $Btu/lb-°F$
$c_{p,c}$	specific heat at constant pressure of coolant, $Btu/lb-°F$
$c_{p,l}$	specific heat at constant pressure of the local air, $Btu/lb-°F$
F	ratio of coolant weight flow rate to local air weight flow rate, $\dfrac{G_c}{(\rho V)_l}$

$$F_\xi = \frac{w/S}{(\rho V)_l}$$

$$f = \frac{\text{Mass loss by vaporization}}{\text{Total mass loss}}$$

G_c	weight flow rate of coolant per unit area of porous nose, lb/ft^2-sec
H	enthalpy, Btu/lb
h	heat-transfer coefficient, $Btu/ft^2-sec-°F$
h_{eff}	effective heat of ablation, Btu/lb
h_{ov}	intrinsic heat capacity, Btu/lb

2

K	thermal conductivity, $Btu/ft^2\text{-sec-}^\circ F/ft$
M	Mach number
N_{Pr}	Prandtl number
N_{St}	Stanton number
p	pressure, lb/sq ft
p_{cone}	cone pressure, lb/sq ft
$p_{t,2}$	total pressure behind normal shock, lb/sq ft
Δp	pressure drop across porous nose cap, lb/sq ft
q	heat flux, $Btu/ft^2\text{-sec}$
r	nose radius, ft
S	cooled area downstream of porous nose, sq ft
s	distance downstream from porous nose-cap-conical-afterbody juncture, in.
T	temperature, $^\circ F$
$\overline{T}$	average temperature
t	time, sec
V	velocity, ft/sec
w	coolant flow rate, lb/sec
x	distance along porous nose cap from stagnation point, ft
ρ	density, lb/cu ft
τ	skin thickness, ft

Subscripts:

air	air
aw	adiabatic wall
c	coolant
cone	cone

ch	chamber
eq	equilibrium or steady-state
l	local
pw	porous wall
r	boundary-layer recovery value with coolant flow
s	outside surface
sl	sea level
sw	solid-wall
t	stagnation
tr	transient
w	inside surface
∞	free-stream
0	theory for no coolant flow

MODEL AND TEST

Model Configuration and Cooling System

The model was a body of revolution 38 inches long having a blunted porous nose with a 6° half-angle cone-cylinder afterbody. A photograph of the model and fourth-stage rocket motor is shown in figure 1.

A schematic diagram of the model and cooling system is shown in figure 2. Nitrogen coolant was stored in a cylindrical accumulator at a gage pressure of 2,800 pounds per square inch and was kept in check by means of a squib-actuated valve. Briefly, the normally closed valve holds pressure with no leakage by its solid diaphragm which is machined as an integral part of the valve body. The diaphragm is sheared out by ignition of the squib and allows nitrogen coolant to flow unobstructed through the valve. A flow regulator was used to throttle the nitrogen coolant from the accumulator pressure to the working pressure.

The technique employed in determining the nitrogen coolant flow rate through the stagnation point of the porous nose during flight involved calculating the pressure on the outside surface of the porous nose and the pressure drop Δp through the porous material. A calibration was made in a pressure-vacuum chamber which correlated these two variables with the flow rate as measured by the orifice (fig. 2) installed in the cooling system. During the

4

calibration procedure the explosive valve (fig. 2) was replaced with a solenoid-operated gate valve in order to facilitate the operation. The resulting calibration curves are shown in figure 3.

Model Construction and Instrumentation

Figure 4 is a sketch of the model showing the pertinent construction details and dimensions. The 4-inch-diameter porous nose cap through which the coolant passed was formed from 347 sintered powdered stainless-steel sheet 0.093 inch in thickness to a ratio of nose radius to radius of curvature of 1/3. The porous nose cap was fastened to the stainless-steel nose chamber by means of welded butt joints. The 6° conical afterbody consisted of an outer skin and an inner heat shield. The outer skin was rolled from Inconel sheet 0.078 inch in thickness and the heat shield was rolled from 0.050-inch stainless-steel sheet. The two conical sections were fastened to two SAE 4340 steel rings by welded-lap joints. The nose chamber and 6° conical afterbody were fastened together with flat-head machine screws.

A 10-channel telemeter which was located just behind the cooling system (fig. 2) transmitted four channels of pressure, two channels of temperature, and one channel each of normal, transverse, thrust, and drag accelerations. Twenty No. 30 gage chromel-alumel thermocouples were installed in the model at the locations shown in figure 4. Eleven of these were spotwelded to the back side of the conical skin. Seven were spotwelded to the back side of the porous nose cap through which the coolant passed. Two thermocouples (thermocouples 8 and 9) were used for measuring nitrogen coolant temperature and were located in the nose chamber and at the flow measuring orifice, respectively, as shown in figure 4.

Four pressure orifices were installed in the model at the locations shown in figure 4. One of these was located on the bulkhead inside the nose chamber and was used to measure the chamber pressure. Two pressure orifices (orifices 2 and 3) were used for measuring the total coolant flow rate and were located at the flow measuring orifice. The fourth pressure orifice was located on the aft portion of the conical skin and was used for measuring surface pressure.

Other instrumentation consisted of ground-based radar units for measuring model velocity and for obtaining the location of the model in space.

Atmospheric data and wind conditions were measured to an altitude of 90,000 feet by means of a radiosonde launched near the time of flight and tracked by Rawin set AN/GMD-1A.

Propulsion System

The propulsion system consisted of four stages of solid-propellant rocket motors. The first and second stages were an Honest John rocket motor and a Nike rocket motor, respectively. The third and fourth stages were a Lance rocket motor and a Recruit rocket motor, respectively. A photograph of the model and propulsion system is shown in figure 5.

Flight-Test Procedure

The model was ground launched at an elevation angle of 72°. A plot of the flight trajectory and the sequence of events are shown in figure 6. The first-stage rocket motor burned for approximately 5 seconds, drag separated immediately, and allowed the remaining three stages to coast to the desired second-stage ignition time. The second-stage rocket motor was fired at 15.2 seconds by a mechanical timer and burned for about 3.2 seconds. A coast period of approximately 53 seconds followed and allowed the vehicle to reach the test altitude. At 71.1 seconds the third-stage rocket motor was fired by the timer and at the same time the nitrogen cooling system was actuated. At the third-stage burnout (77.5 seconds) the fourth-stage rocket motor was fired by the timer and burned for about 2 seconds. A partial telemeter failure occurred at 77.5 seconds and complete failure of the telemeter signal occurred at 79.0 seconds.

The variation of flight velocity and altitude as determined from the radar data is shown in figure 7. Time histories of the free-stream temperature and pressure obtained from the radiosonde and flight trajectory measurements are shown in figure 8. Variation of the free-stream Mach number and free-stream Reynolds number per foot for the flight trajectory is shown in figure 9.

RESULTS AND DISCUSSION

Pressure and Flow Data

Figure 10 presents the ratio of the measured surface pressure on the conical afterbody to the calculated stagnation pressure on the nose cap. For comparison the ratio of the theoretical pressure for a sharp 6° half-angle cone from reference 4 to the calculated stagnation pressure on the nose cap is also presented. The measured pressure is somewhat greater than the theoretical sharp cone pressure. At 77.5 seconds (ignition of fourth-stage motor), a partial failure in the telemetry system occurred; consequently, no cone surface-pressure data were available beyond this time.

The measured chamber pressure and the calculated surface pressure at the stagnation point are shown in figure 11(a) as a function of time. Figure 11(b) shows the flow rate of nitrogen coolant through the stagnation point of the porous nose cap during the flight test which was determined from the data of figure 11(a) and the calibration curves shown in figure 3. As mentioned previously, the calibration procedure correlated the coolant flow rate with both the pressure drop across the porous nose cap Δp and the nose surface pressure. In addition to these two variables the coolant flow rate was also a function of the coolant density. Since the coolant was injected through the porous nose at a temperature different from that during the calibration procedure, a correction was necessary. This correction was accomplished by multiplying the flow rate obtained from figure 3 by the ratio of the average coolant density passing through the porous nose in flight to the density of the coolant during the calibration tests. No attempt was made to correct the coolant flow rate for viscous effects and inertial resistance.

6

Temperature Data

The measured temperature distributions on both the porous nose cap and the nonporous conical afterbody are shown in figures 12 and 13, respectively. Examination of the data indicates fairly symmetrical heating on both the nose and afterbody during the flight data period. Typical time histories of the measured inside surface temperature and the computed outside surface temperature for both the porous nose cap and the nonporous conical afterbody are presented in figures 14(a) and 14(b), respectively. At the beginning of the data period when the heat input was relatively low, no temperature gradient existed through either the porous nose cap or the nonporous conical afterbody. Since the coolant temperature was much lower than the porous nose cap temperature, a sharp decrease in the wall temperature occurred during the first few seconds of the data period. However, during the latter portion of the data period the heat input was very high and, as a result, a temperature gradient existed through both the porous nose cap and the nonporous conical afterbody. Details of the procedure for calculating the temperature gradients through the porous nose and the nonporous conical afterbody are described in the appendix and in reference 5, respectively.

Heat Transfer

From the appendix the general heat balance equation on the porous nose cap is given as

$$h(T_r - T_s) = G_c c_{p,c}(T_s - T_c) + \left[\rho \tau c \left(\frac{dT_w}{dt}\right)\right]_{pw}$$

where both radiation from and conduction along the porous nose cap have been neglected. Dividing this equation by $h_o(T_r - T_s)$ results in the following relation:

$$\frac{h}{h_o} = \frac{G_c c_{p,c}(T_s - T_c)}{h_o(T_r - T_s)} + \frac{\left[\rho \tau c \left(\frac{dT_w}{dt}\right)\right]_{pw}}{h_o(T_r - T_s)}$$

Since the ratio h/h_o is analogous to the ratio $N_{St}/N_{St,o}$, this equation shows the heat reduction or shielding effect of transpiration. The heat-transfer coefficient h_o for no coolant flow was computed from $h_o = \frac{q_t c_{p,l}}{H_t - H_s}$ where the quantity $c_{p,l}$ was the average specific heat through the boundary layer which was calculated from the relation $c_{p,l} = \frac{H_l - H_s}{T_l - T_s}$ according to the appendix of

7

reference 6. The quantity q_t was the stagnation-point heat input computed from the following empirical equation given in reference 7:

$$q_t = \left(\frac{17,600}{\sqrt{r}}\right)\sqrt{\frac{\rho_\infty}{\rho_{sl}}}\left(\frac{V_\infty}{26,000}\right)^{3.15}\left[\frac{H_{aw} - H_s}{H_{aw} - (H_s)_{540° R}}\right]$$

Figure 15 shows a plot of q_t computed from the preceding relation which was corrected for the bluntness of the nose cap according to figure 3 of reference 8.

Figure 16 shows a plot of the shielding effect or heat reduction at the stagnation point of the porous nose cap where the ratio $N_{St}/N_{St,0}$ is expressed as a function of the flow parameter $\dfrac{F}{N_{St,0}}\dfrac{c_{p,c}}{c_{p,l}}\left(\dfrac{T_l}{T_s}\right)^{0.21}$ for the high-heat-input portion of the flight. Also shown are the theoretical results from reference 9 for a three-dimensional laminar stagnation boundary layer which were transformed to the parameters used in the present investigation by the procedure given in reference 6. The theoretical results given in reference 9 were for several values of the ratio of T_l/T_s ranging from 1/4 to 4; however, when the flow parameter $\dfrac{G_c c_{p,c}}{h_0}$, or nondimensionally $\dfrac{F}{N_{St,0}}\dfrac{c_{p,c}}{c_{p,l}}$, was multiplied by the ratio of $(T_l/T_s)^{0.21}$, the values of $N_{St}/N_{St,0}$ all fell on a single curve as shown in figure 16. Thus, the ratio $(T_l/T_s)^{0.21}$ is a correlation factor when included in the nondimensional flow-rate parameter. It permits transpiration results with values of T_l/T_s either greater or less than 1 to be plotted on a single curve. The theoretical analysis of Reshotko and Cohen (ref. 10) for a three-dimensional laminar stagnation boundary layer was correlated in the same manner by the authors of reference 6; however, the correlation factor was found to be $(T_l/T_s)^{0.19}$. For comparison the theoretical results of reference 10 for T_l/T_s equal to 1.0 are shown.

The shaded circular symbol in figure 16 represents the time at which $\left(\dfrac{dT_w}{dt}\right)_{pw}$ is equal to zero. At this time quasi-steady-state or equilibrium conditions exist; hence the outside surface temperature can be computed by using the equilibrium relations. (See appendix.) At other times the solutions for T_s are approximate since transient conditions exist. The shaded symbol therefore serves as a datum point to substantiate the validity of the approximate method for computing the transient surface temperature.

Examination of the flight data in figure 16 shows a heat-transfer reduction due to transpiration of approximately two orders of magnitude at the stagnation point of the porous nose cap. The present results with large rates of mass injection appear to be a reasonable correlation with theory for relatively low and moderate rates of mass injection by including the temperature ratio in the nondimensional flow-rate parameter. The ratio T_l/T_s extended over a range from 5.85 to 11.01 during the high-heat-input portion of the flight data period.

If ablating materials are to be used to provide heat protection for spacecraft reentering the earth's atmosphere, knowledge of the shielding effect to high velocities is required. As pointed out in reference 6, the expressions relating the ablation parameters for a noncharring ablator to the material and boundary-layer characteristics may be derived from transpiration cooling results. Figure 17 shows the effective heat of ablation as a function of the enthalpy parameter for a three-dimensional laminar stagnation boundary layer which was derived from the transpiration results of figure 16. Also shown are the theoretical results from reference 9. An experimental datum point from an arc-jet test on a subliming ablation material taken from reference 11 is also shown. The enthalpy parameter for the test of reference 11 was evaluated by using 900 Btu/lb, 0.5, and 5.98 for the quantities h_{ov}, $c_{p,c}/c_{p,l}$, and T_l/T_s, respectively, (from ref. 6) where h_{ov}, the intrinsic heat capacity, is defined as the heat absorbing capacity of an ablation material from its starting temperature through melting (if the material melts first) and vaporization. The f factor which is the ratio of mass loss by vaporization to the total mass loss was assumed to be equal to 1.0. The flight velocity corresponding to the enthalpy level for the data of reference 11 is approximately 18,000 feet per second which is about the maximum value that has been obtained experimentally in either free flight or ground test facilities. A line is shown in figure 17 at a value of 32 for the enthalpy parameter to indicate the area of planetary reentry where h_{ov} was arbitrarily chosen to be equal to 1,000 Btu/lb and the product of the f factor, the specific heat ratio, and temperature ratio to be equal to 1.0. Since the values of the enthalpy parameter obtained from transformed transpiration results are proportional to the mass-injection rate, large rates of mass injection for a transpiration test simulate a high velocity for an ablation test. Thus, the transformation of the present transpiration cooling data to ablation parameters permits an extension of theory and experimental ground tests results to supercircular velocities for subliming ablation materials.

Figure 18 shows the variation of the downstream cooling temperature parameter $\left(\dfrac{T_s - T_c}{T_{aw} - T_c}\right)_{eq}$ on the conical afterbody as a function of the flow parameter $\dfrac{F_\xi}{N_{St,0}} \dfrac{c_{p,c}}{c_{p,l}}$ for the Mach number variation from 3.81 to 6.15 and over a local Reynolds number per foot range from 3.98×10^5 to 5.30×10^5. The nondimensional flow rate F_ξ was computed from $F_\xi = \dfrac{w/S}{(\rho V)_l}$ where w was the flow rate

of coolant in pounds per second and S was the skin area from the porous nose-cap-conical-afterbody juncture to the downstream thermocouple stations. Included for comparison is a curve representing the data of reference 2 for a turbulent boundary layer with a zero-pressure gradient at a Mach number of 2.0. The equation for computing the equilibrium downstream cooling temperature parameter $\dfrac{T_s - T_c}{T_{aw} - T_c}$ from the transient flight data (from ref. 6):

$$\left(\frac{T_s - T_c}{T_{aw} - T_c}\right)_{eq} = \left(\frac{T_s - T_c}{T_{aw} - T_c}\right)_{tr} + \frac{\left(\rho \tau c \, \dfrac{d\overline{T}}{dt}\right)_{sw}}{h_o(T_{aw} - T_c)\left(\dfrac{N_{St}}{N_{St,0}} + \dfrac{F_\xi}{N_{St,0}} \dfrac{c_{p,c}}{c_{p,l}}\right)}$$

modified for convenience to the form:

$$\left(\frac{T_s - T_c}{T_{aw} - T_c}\right)_{eq} = \left(\frac{T_s - T_c}{T_{aw} - T_c}\right)_{tr} + \frac{\left(\rho \tau c \, \dfrac{d\overline{T}}{dt}\right)_{sw}\left(T_{aw} - T_s\right)_{eq}}{G_c c_{p,c}(T_{aw} - T_c)^2}$$

was solved by an iteration process. The value T_{aw}, the boundary-layer recovery temperature for no coolant flow, was calculated from the relation

$$T_{aw} = N_{Pr}^{1/2}(T_t - T_l) + T_l$$

The values of $N_{St,0}$ were calculated according to the theory of Van Driest for a laminar boundary layer from reference 12 by using the local conditions computed by the conical-theory methods of reference 13 using the theoretical values for p_{cone}. The boundary layer is assumed to be laminar since the data thus evaluated fall within a reasonable range of the results of reference 2 shown in figure 18. If the flow parameter were evaluated by using a turbulent value of $N_{St,0}$ the present data would have fallen considerably to the left of the laminar results shown in figure 18 which would appear to be unreasonably inconsistent. Furthermore, the local Reynolds number at thermocouple station 20 never exceeded 1.0×10^6.

The parameters used in figure 18 correlate the downstream cooling data well up through 77 seconds. The Mach number and Reynolds number variation with time appear to have no significant effect on the correlation. Examination of the data shows a substantial reduction of the equilibrium wall temperature on the conical afterbody, the greater reduction occurring near the nose cap. Comparison of the present data with the results of reference 2 indicates that, for the same coolant flow rate, lower surface temperatures are achieved in a laminar boundary layer than in a turbulent boundary layer.

10

Beyond 77.0 seconds the data were disregarded because the coolant temperature could not be determined accurately. The coolant temperature was assumed to be equal to the surface temperature at the porous nose-cap-conical-afterbody juncture which was determined from extrapolating the porous nose temperature distribution curve. From 75.0 seconds to 77.0 seconds the temperature distribution was linear; however, beyond 77.0 seconds a nonlinear temperature distribution existed and, as a consequence, an accurate estimation of the coolant temperature could not be determined.

CONCLUDING REMARKS

Mass-transfer cooling parameters are presented for both a porous stagnation point and a nonporous conical afterbody of a blunted cone in free flight to a maximum Mach number of 10.6 with nitrogen as the coolant.

With large rates of mass injection used in the present investigation, the laminar heat-transfer reduction was approximately two orders of magnitude on the porous nose. The present results appear to be a reasonable correlation with theory for a laminar boundary layer with low and moderate rates of mass injection.

A laminar boundary layer was maintained over the conical afterbody of the blunted cone with mass injection at the stagnation point. A substantial reduction of the equilibrium wall temperature was achieved, the greater reduction occurring near the nose cap. The Mach number and Reynolds number variation with time appear to have no significant effect on the correlation of the data.

The transformation of present mass-transfer results to ablation parameters provides effective heats of ablation for any subliming ablator in a three-dimensional laminar stagnation boundary layer to supercircular velocities.

Langley Research Center,
National Aeronautics and Space Administration,
Langley Station, Hampton, Va., November 15, 1963.

11

APPENDIX

DETERMINATION OF POROUS SURFACE TEMPERATURE

In this section, details of the procedure for calculating the outside surface temperature on the porous nose specimen are presented. From reference 14 the temperature difference between the outside and inside surfaces for equilibrium conditions is given by the equation

$$\frac{T_s - T_w}{T_r - T_c} = \frac{\dfrac{N_{St}c_{p,l}}{Fc_{p,c}}}{1 + \dfrac{N_{St}c_{p,l}}{Fc_{p,c}}}\left[1 - \exp\left(-\frac{G_c c_{p,c}\tau}{K_{pw}}\right)\right] \tag{1}$$

Upon rearrangement, equation (1) can be written as

$$\frac{T_s - T_w}{T_r - T_c} = \frac{\dfrac{\dfrac{N_{St}}{N_{St,0}}}{\dfrac{F}{N_{St,0}}\dfrac{c_{p,c}}{c_{p,l}}}}{1 + \dfrac{\dfrac{N_{St}}{N_{St,0}}}{\dfrac{F}{N_{St,0}}\dfrac{c_{p,c}}{c_{p,l}}}}\left[1 - \exp\left(-\frac{G_c c_{p,c}\tau}{K_{pw}}\right)\right] \tag{2}$$

If both radiation from and conduction along the porous specimen are neglected, the general heat balance equation for transient or nonequilibrium conditions can be written as (from ref. 1):

$$q_{aerodynamic} = q_{absorbed\ by\ coolant} + q_{transient}$$

or

$$h(T_r - T_s) = G_c c_{p,c}(T_s - T_c) + \left(\rho\tau c\,\frac{d\overline{T}}{dt}\right)_{pw}$$

The term $\left(\dfrac{d\overline{T}}{dt}\right)_{pw}$ in the preceding equation is the slope of the curve of average wall temperature against time. Since the temperature gradient through the thickness of the porous nose is unknown, the value of $\left(\dfrac{d\overline{T}}{dt}\right)_{pw}$ cannot be determined; however, since most of the temperature rise occurs very near the hot side of the porous nose according to the results reported in reference 15, the term $\left(\dfrac{dT_w}{dt}\right)_{pw}$ is believed to be a reasonable approximation. Thus,

$$h(T_r - T_s) = G_c c_{p,c}(T_s - T_c) + \left(\rho\tau c\,\frac{dT_w}{dt}\right)_{pw} \tag{3}$$

Equation (3) in nondimensional form becomes

$$\frac{N_{St}}{N_{St,0}} = \frac{F}{N_{St,0}}\frac{c_{p,c}}{c_{p,l}}\frac{T_s - T_c}{T_r - T_s} + \frac{\left(\rho\tau c\,\frac{dT_w}{dt}\right)_{pw}}{N_{St,0}(\rho V)_l c_{p,l}(T_r - T_s)}$$

Upon rearrangement, this equation becomes

$$\frac{\dfrac{N_{St}}{N_{St,0}}}{\dfrac{F}{N_{St,0}}\dfrac{c_{p,c}}{c_{p,l}}} = \frac{G_c c_{p,c}(T_s - T_c) + \left(\rho\tau c\,\frac{dT_w}{dt}\right)_{pw}}{G_c c_{p,c}(T_r - T_s)} \tag{4}$$

Substituting equation (4) for nonequilibrium conditions into equation (2) for equilibrium conditions results in the following relation which is believed to give an approximate solution for evaluating the outside surface temperature for the range of test conditions presented herein:

$$\frac{T_s - T_w}{T_r - T_c} = \frac{\dfrac{G_c c_{p,c}(T_s - T_c) + \rho\tau c\left(\frac{dT_w}{dt}\right)_{pw}}{G_c c_{p,c}(T_r - T_s)}}{1 + \dfrac{G_c c_{p,c}(T_s - T_c) + \rho\tau c\left(\frac{dT_w}{dt}\right)_{pw}}{G_c c_{p,c}(T_r - T_s)}}\left[1 - \exp\left(-\frac{G_c c_{p,c}\tau}{K_{pw}}\right)\right]$$

The solution of this relation for T_S results in the following equation:

$$T_S = \frac{\left[G_c c_{p,c}(T_r - T_c)\right]\left\{T_w - T_c\left[1 - \exp\left(-\frac{G_c c_{p,c}\tau}{K_{pw}}\right)\right]\right\} + \left(\rho\tau c \frac{dT_w}{dt}\right)_{pw}\left\{T_w + (T_r - T_c)\left[1 - \exp\left(-\frac{G_c c_{p,c}\tau}{K_{pw}}\right)\right]\right\}}{\left[G_c c_{p,c}(T_r - T_c)\right]\left[\exp\left(-\frac{G_c c_{p,c}\tau}{K_{pw}}\right)\right] + \left(\rho\tau c \frac{dT_w}{dt}\right)_{pw}} \quad (5)$$

where T_S is the approximate outside surface temperature for transient or non-equilibrium conditions. If $\left(\dfrac{dT_w}{dt}\right)_{pw} = 0$ in equation (5), the results can be written as

$$T_S = T_c + \frac{T_w - T_c}{\exp\left(-\dfrac{G_c c_{p,c}\tau}{K_{pw}}\right)}$$

which is the exact solution for the porous surface temperature for steady-state or equilibrium conditions.

14

REFERENCES

1. Rashis, Bernard: Exploratory Investigation of Transpiration Cooling of a 40° Double Wedge Using Nitrogen and Helium as Coolants at Stagnation Temperatures From 1,295° F to 2,910° F. NASA TN D-721, 1961.

2. Witte, William G., and Rashis, Bernard: An Experimental Investigation and Correlation of the Heat Reduction to Nonporous Surfaces Behind a Porous Leading Edge Through Which Coolant is Ejected. NASA TM X-235, 1960.

3. Walton, Thomas E., Jr., and Rashis, Bernard: Measurement and Empirical Correlation of Transpiration-Cooling Parameters on a 25° Cone in a Turbulent Boundary Layer in Both Free Flight and a Hot-Gas Jet. NASA TN D-967, 1961.

4. Ames Research Staff: Equations, Tables, and Charts for Compressible Flow. NACA Rep. 1135, 1953. (Supersedes NACA TN 1428.)

5. Hill, P. R.: A Method of Computing the Transient Temperature of Thick Walls From Arbitrary Variation of Adiabatic-Wall Temperature and Heat-Transfer Coefficient. NACA Rep. 1372, 1958. (Supersedes NACA TN 4105.)

6. Rashis, Bernard, and Hopko, Russell N.: An Analytical Investigation of Ablation. NASA TM X-300, 1960.

7. Detra, R. W., Kemp, N. H., and Riddell, F. R.: Addendum to "Heat Transfer to Satellite Vehicles Re-entering the Atmosphere." Jet Propulsion, vol. 27, no. 12, Dec. 1957, pp. 1256-1257.

8. Stoney, William E., Jr.: Aerodynamic Heating of Blunt Nose Shapes at Mach Numbers Up to 14. NACA RM L58E05a, 1958.

9. Howe, John T., and Mersman, William A.: Solutions of the Laminar Compressible Boundary-Layer Equations With Transpiration Which are Applicable to the Stagnation Regions of Axisymmetric Blunt Bodies. NASA TN D-12, 1959.

10. Reshotko, Eli, and Cohen, Clarence B.: Heat Transfer at the Forward Stagnation Point of Blunt Bodies. NACA TN 3513, 1955.

11. Rashis, Bernard, and Walton, Thomas E., Jr.: An Experimental Investigation of Ablating Materials at Low and High Enthalpy Potentials. NASA TM X-263, 1960.

12. Van Driest, E. R.: Investigation of Laminar Boundary Layer in Compressible Fluids Using the Crocco Method. NACA TN 2597, 1952.

13. Moeckel, W. E.: Some Effects of Bluntness on Boundary-Layer Transition and Heat Transfer at Supersonic Speeds. NACA Rep. 1312, 1957. (Supersedes NACA TN 3653.)

14. Hyman, Seymour C.: A Note on Transpiration Cooling. Jet Propulsion, vol. 26, no. 9, Sept. 1956, p. 780.

15. Beusman, C.: Feasibility Study of Transpiration Cooling for the Mark II Polaris Re-Entry Body - Period From 11 November 1958 to 11 May 1959. NDA 2110-6 (Subcontract NOrd 17017), Nuclear Dev. Corp. of America, May 11, 1959.
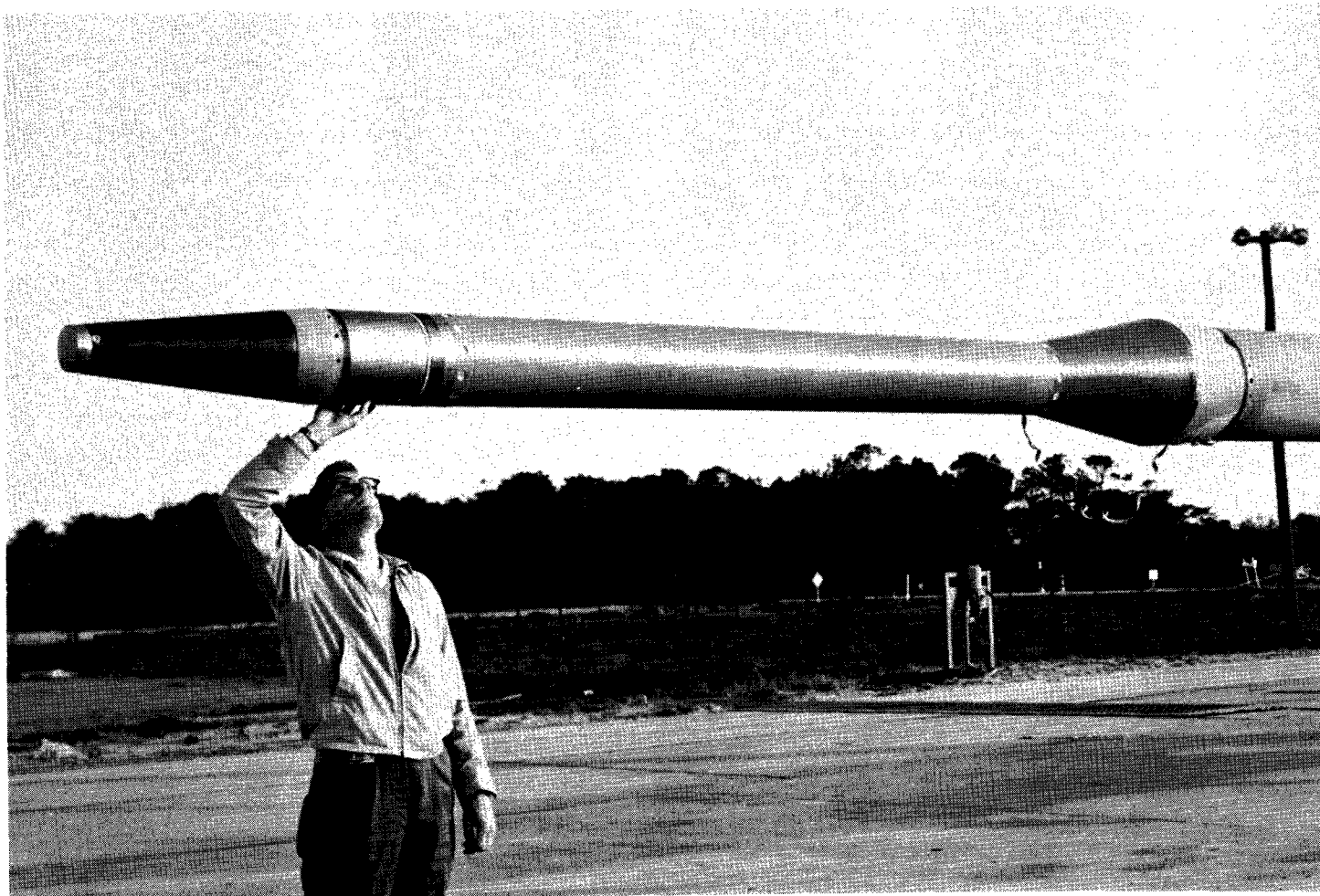
Figure 1.- Photograph of model and fourth stage.

Station 0   Station 25.0"   Station 38.0"

Nose   Flow
chamber   regulator

6°

Accumu-   Telemeter   Recruit
lator   package   motor

Porous   Flow measuring   Squib-actuated
nose cap   orifice   valve
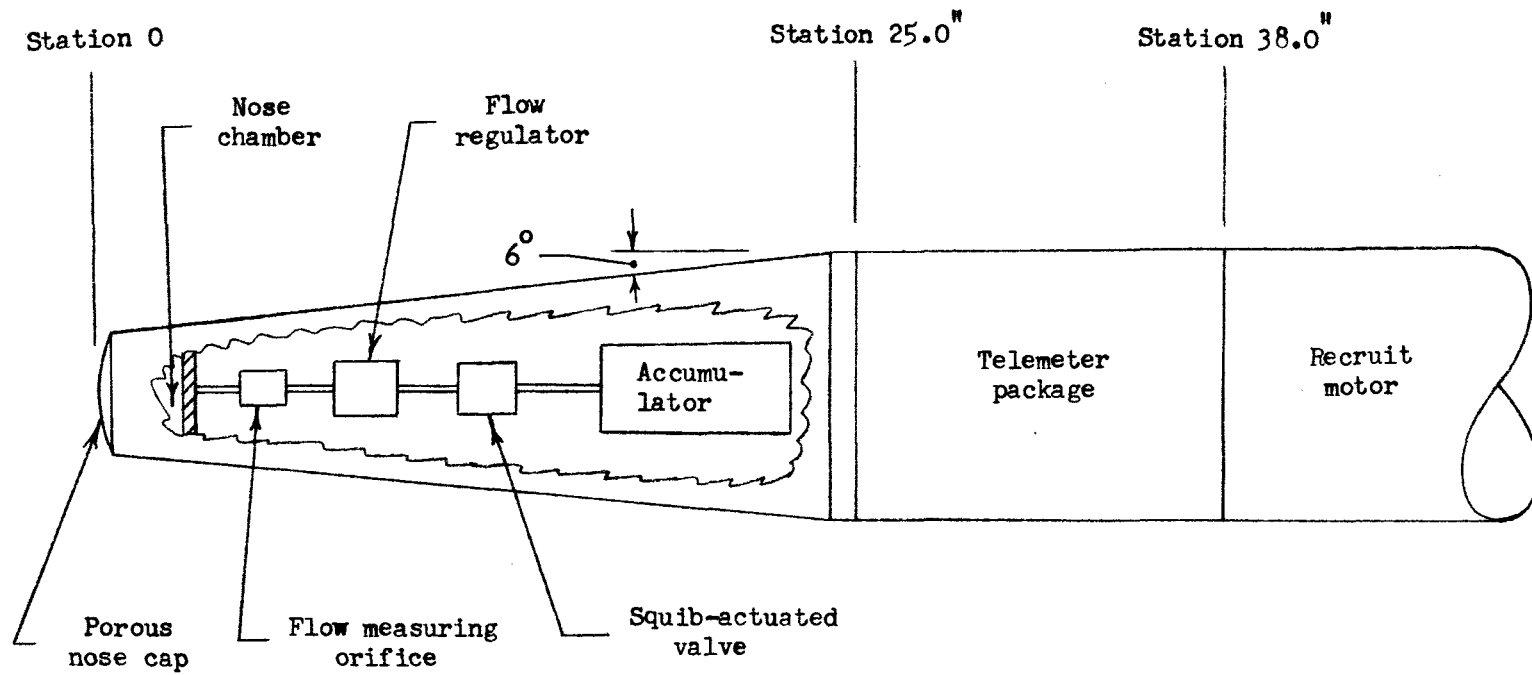
Figure 2.- Schematic diagram of model showing nitrogen cooling system.
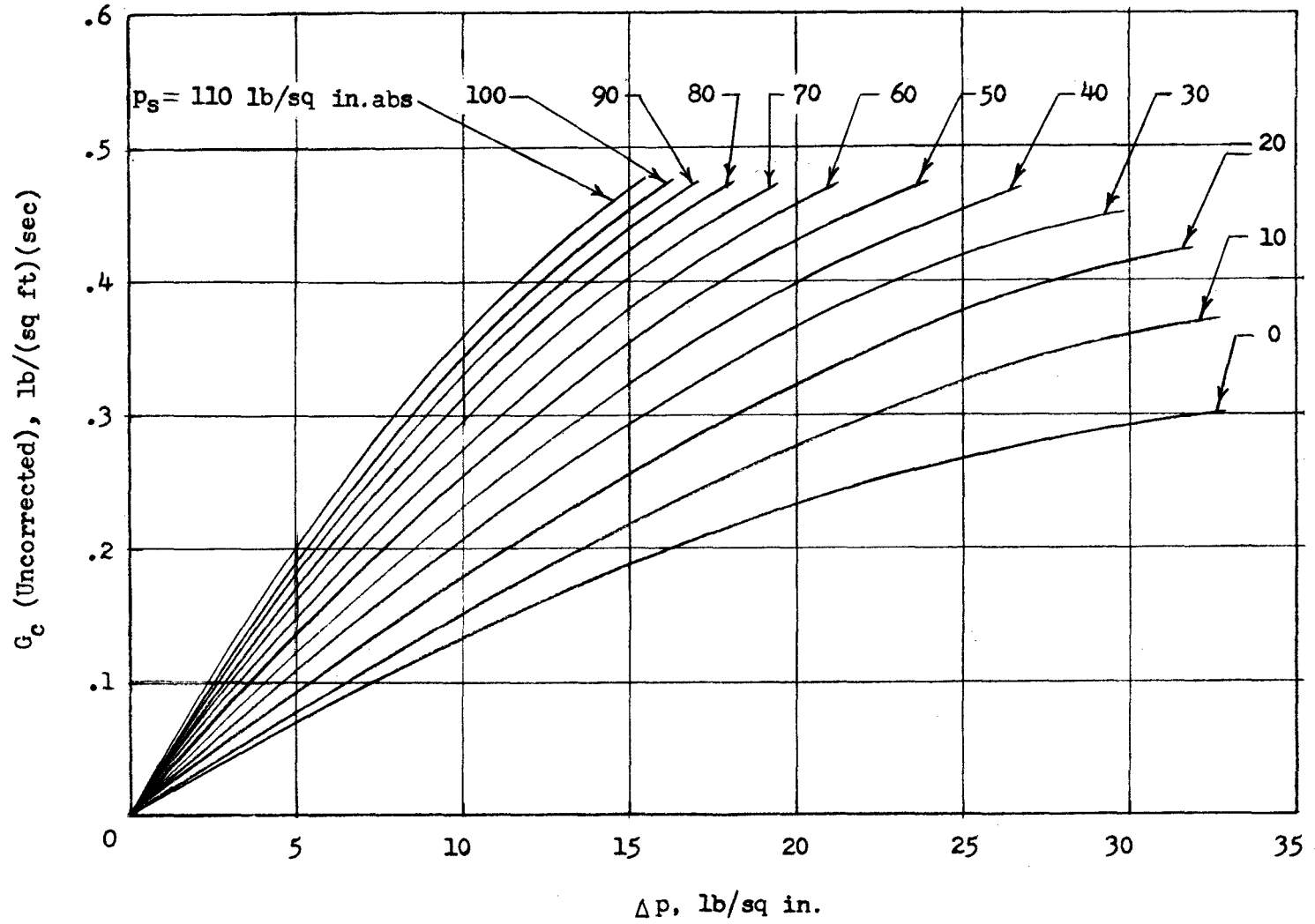
Figure 3.- Flow rate of nitrogen coolant as a function of Δp for several surface pressures on porous nose.
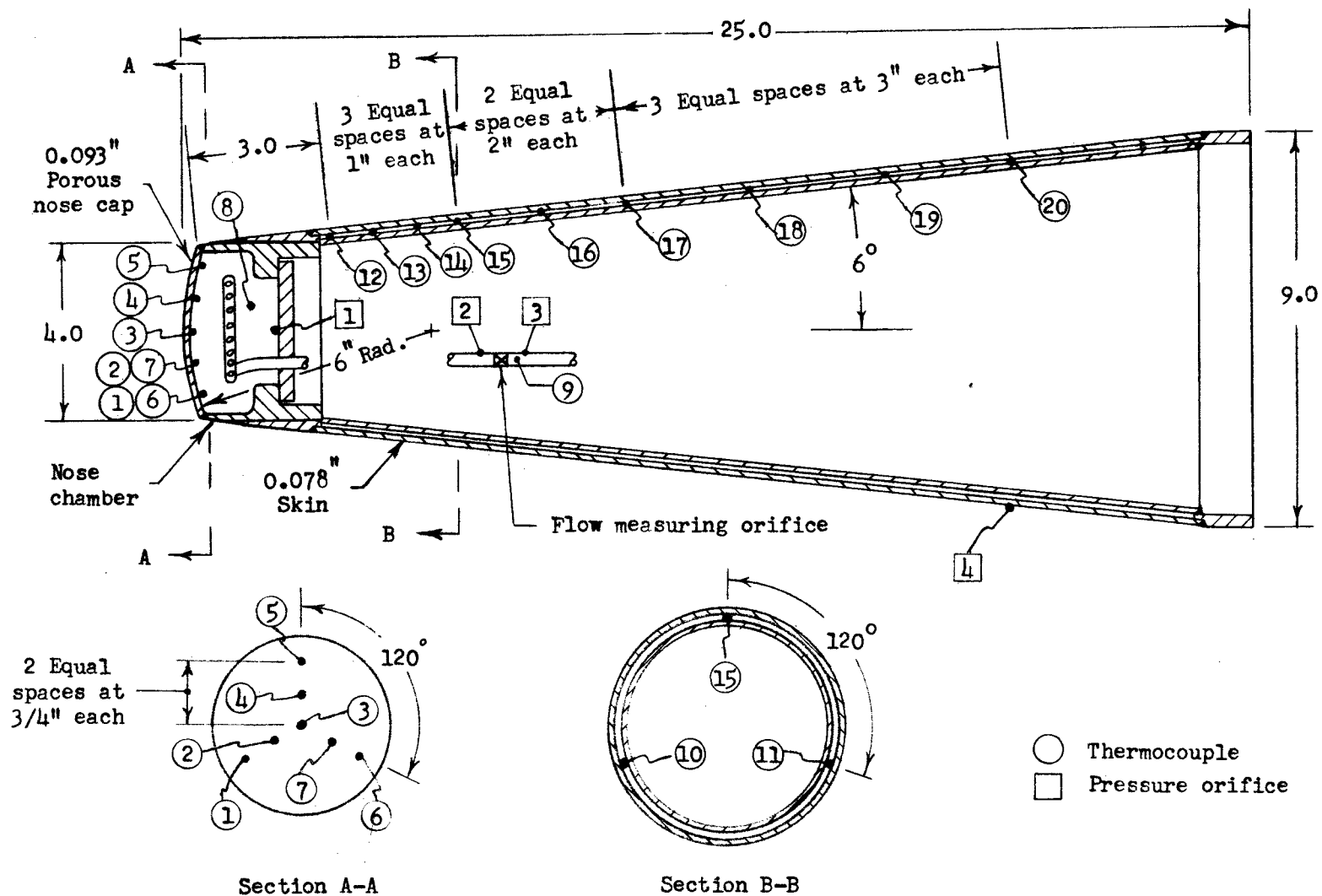
Figure 4.- Sketch of model cone showing construction details and location of instrumentation. All dimensions are in inches.
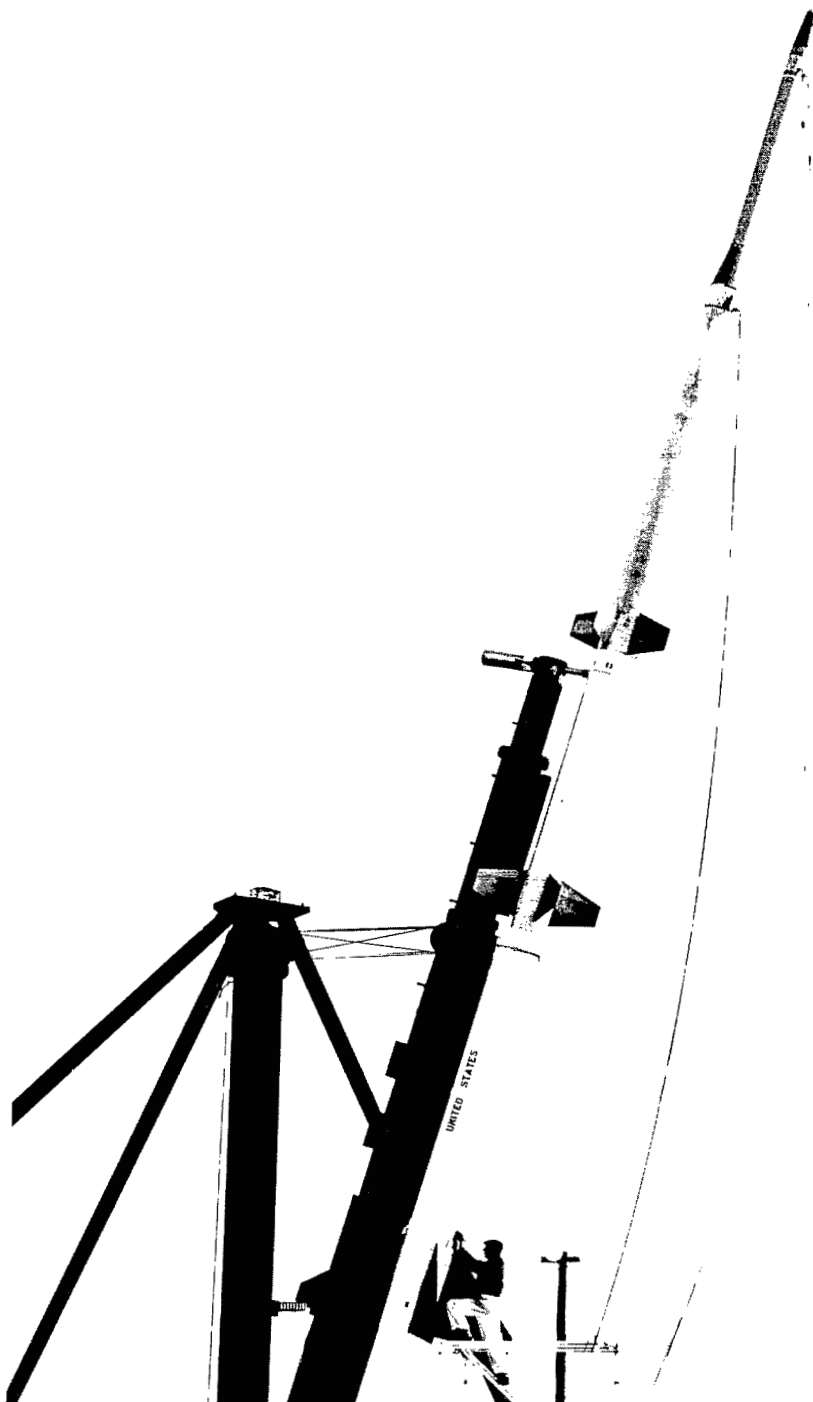
Figure 5.- Photograph of model and booster on launcher.   L-62-3341
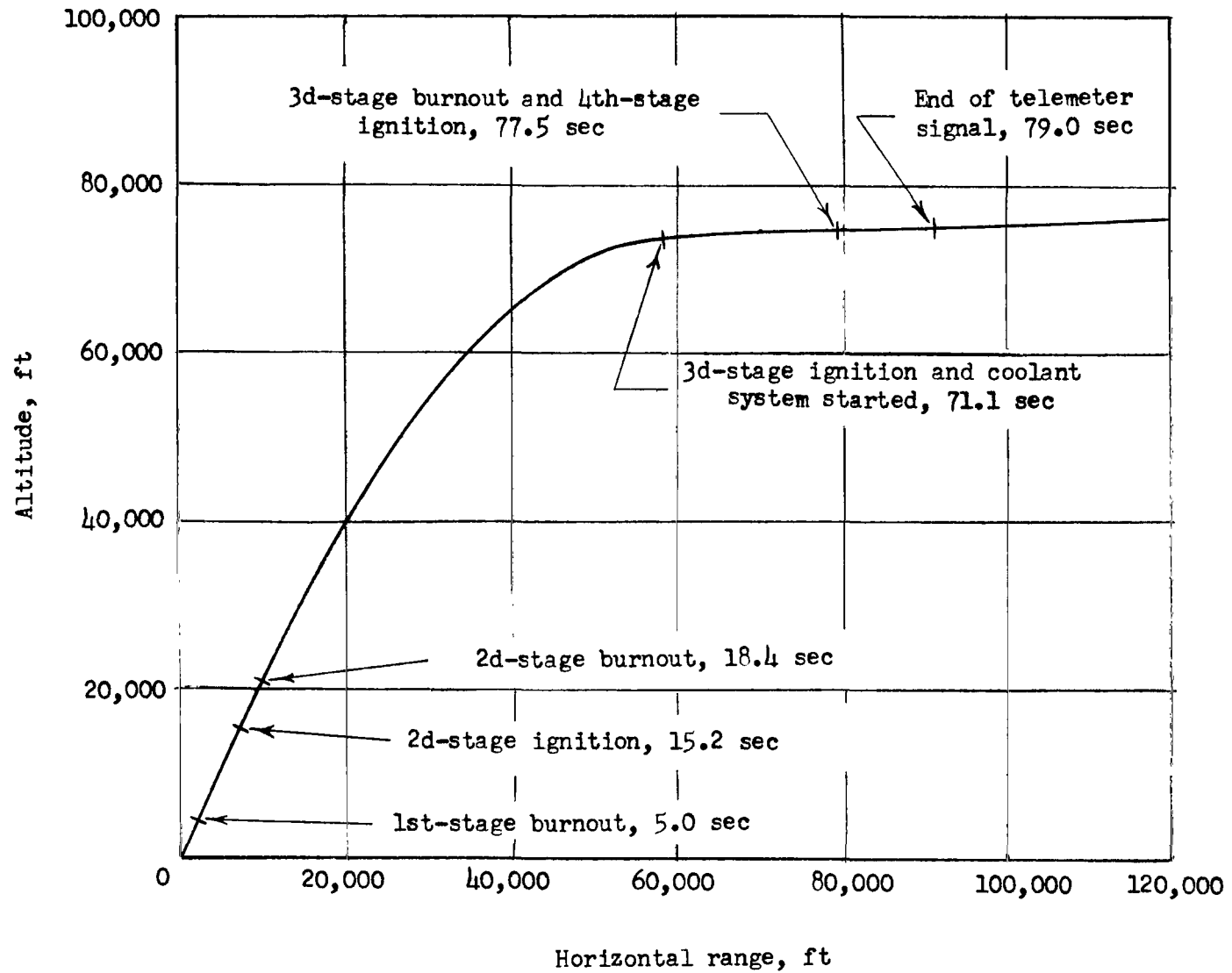
Figure 6.- Flight trajectory.
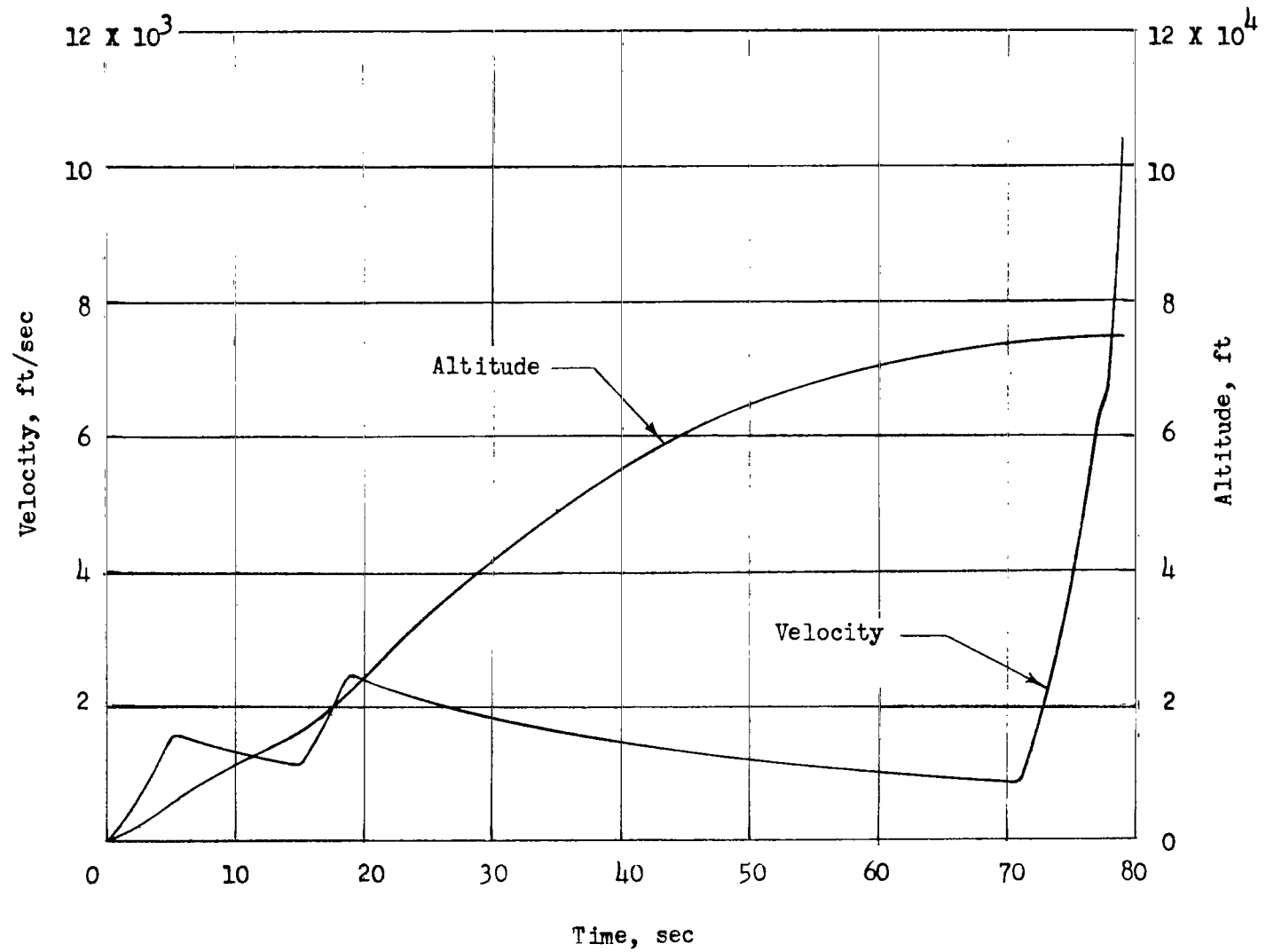
Figure 7.- Velocity and altitude for model flight trajectory.
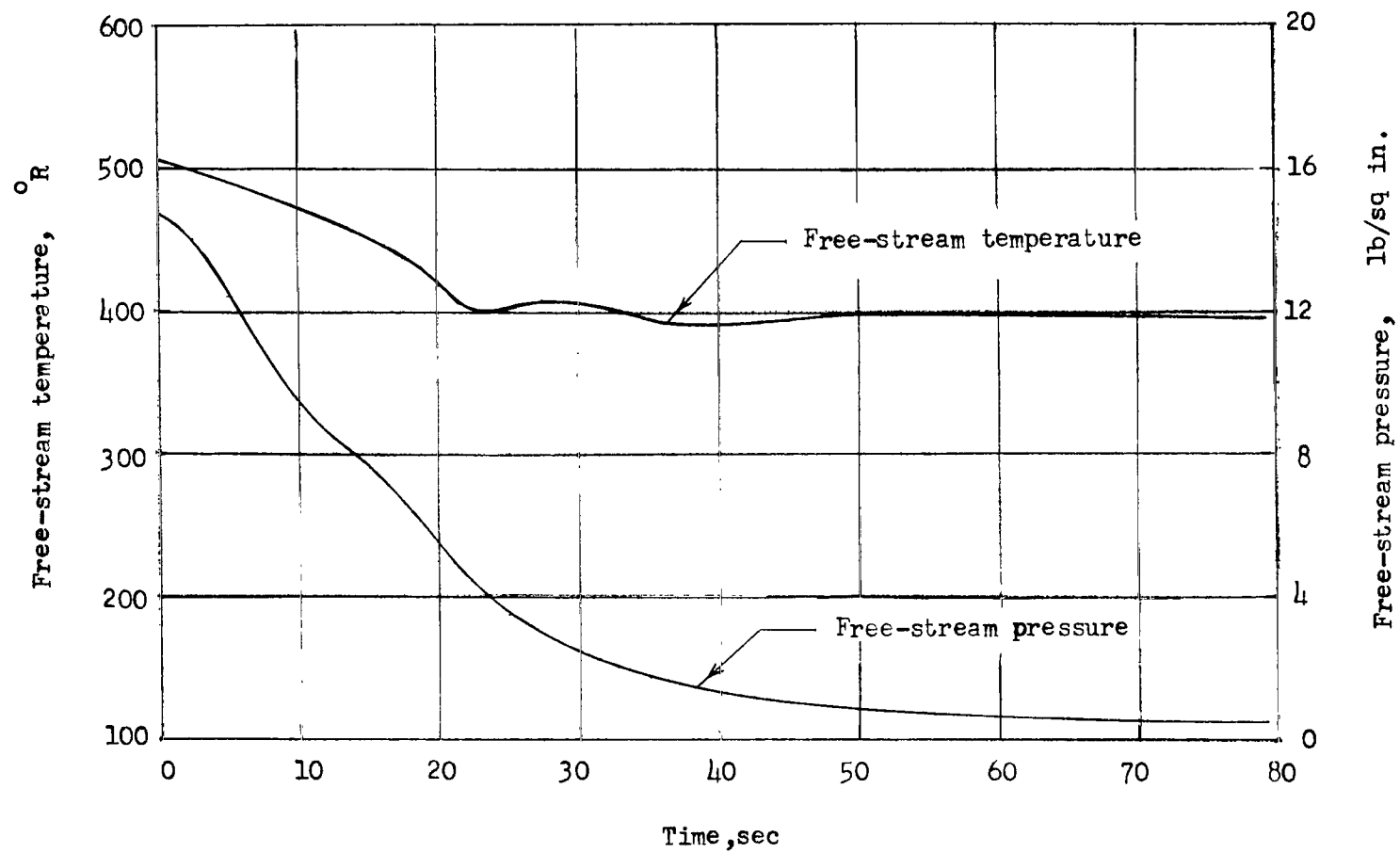
Figure 8.- Free-stream temperature and free-stream pressure for model flight trajectory.
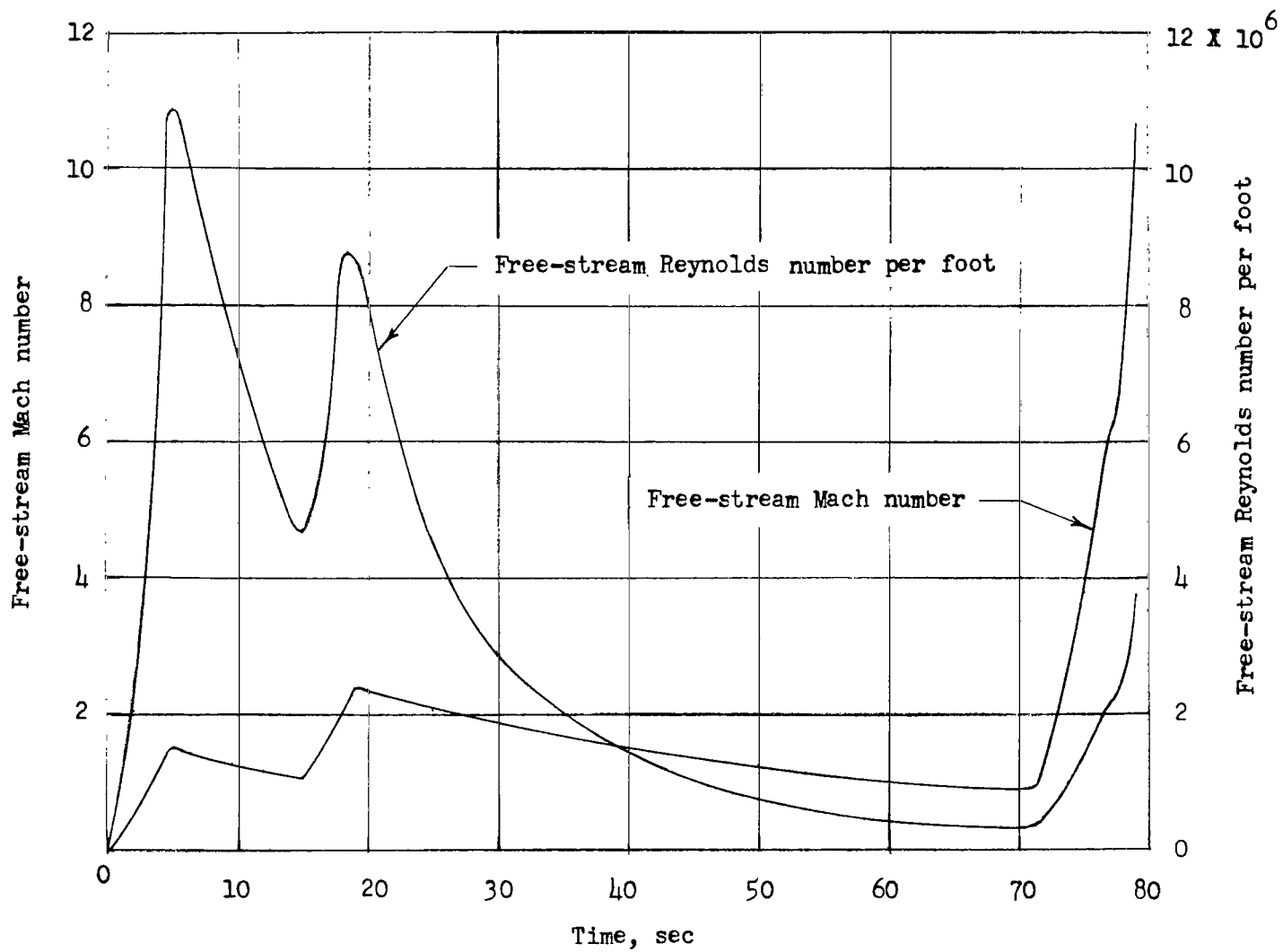
Figure 9.- Free-stream Mach number and free-stream Reynolds number per foot for model flight trajectory.
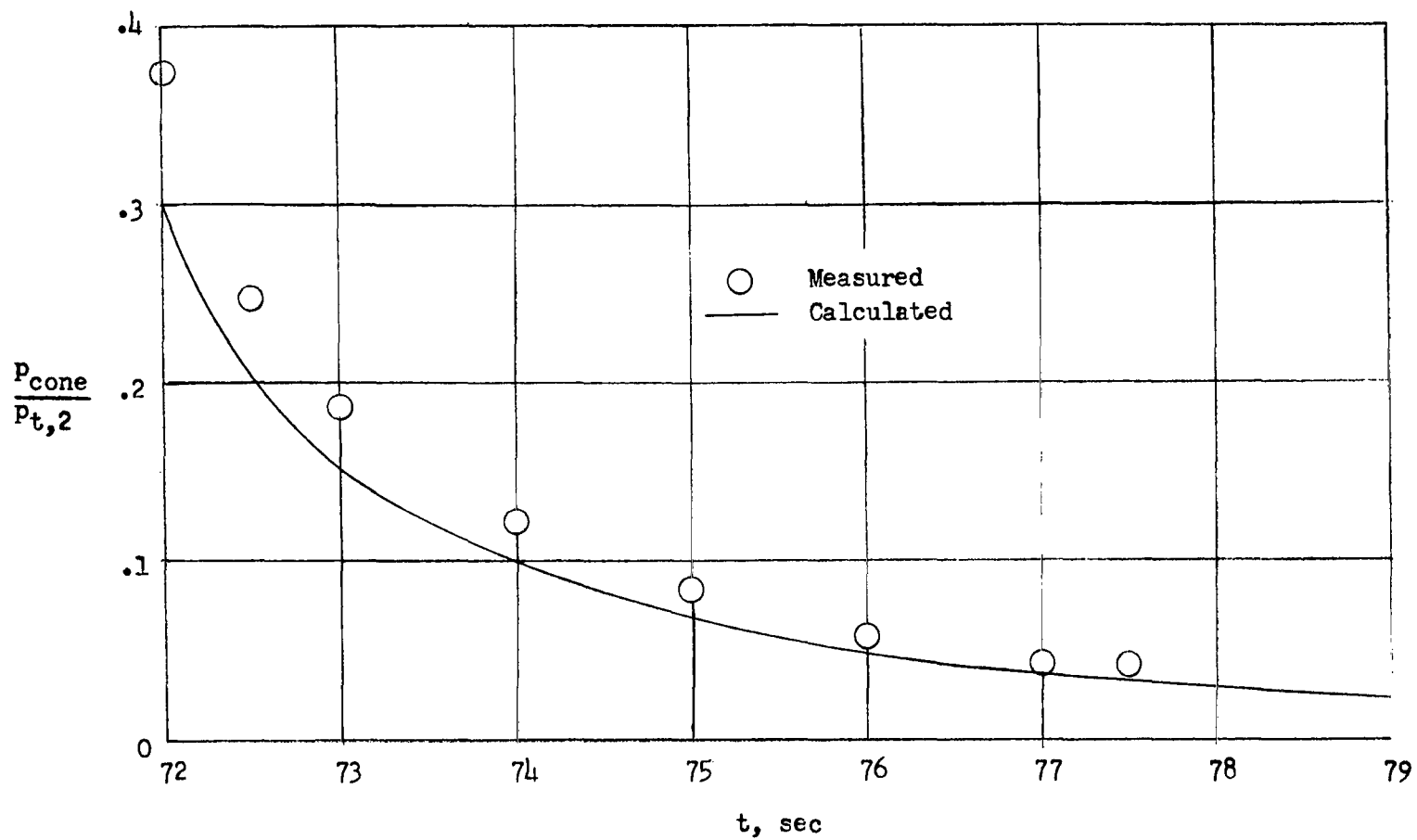
Figure 10.- Ratio of cone pressure to stagnation pressure as a function of time.
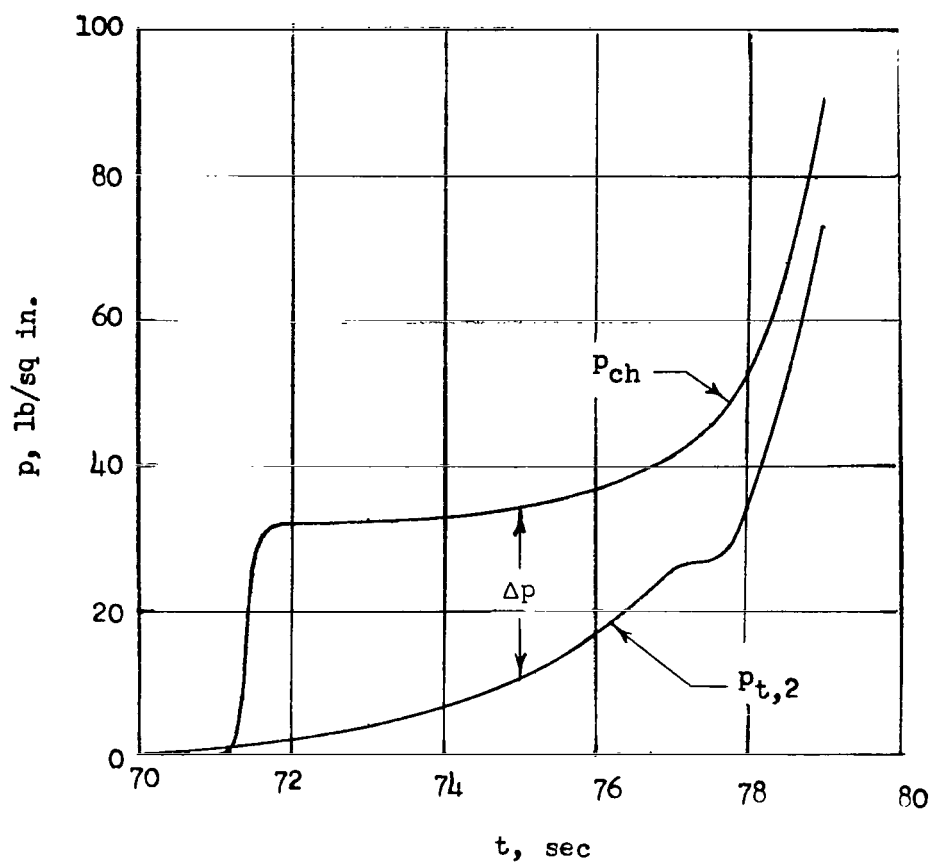
(a) Chamber pressure, stagnation point surface pressure, and Δp on the porous nose.
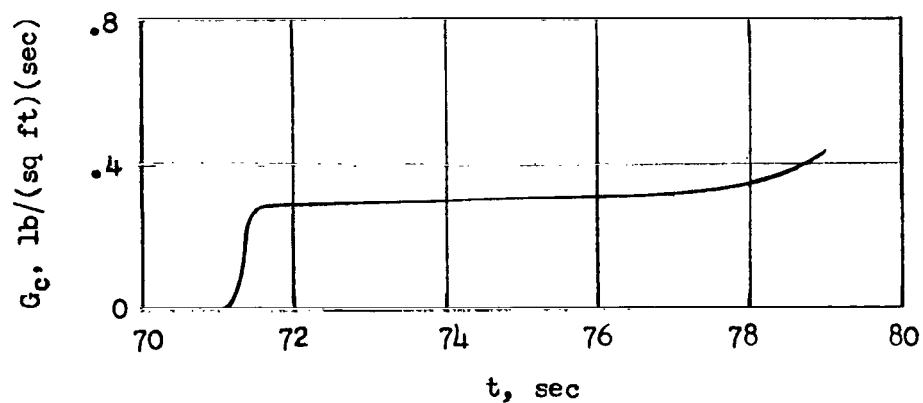
(b) Flow rate of nitrogen coolant at stagnation point.

Figure 11.- Flight model pressures and coolant flow rate at stagnation point as a function of time.
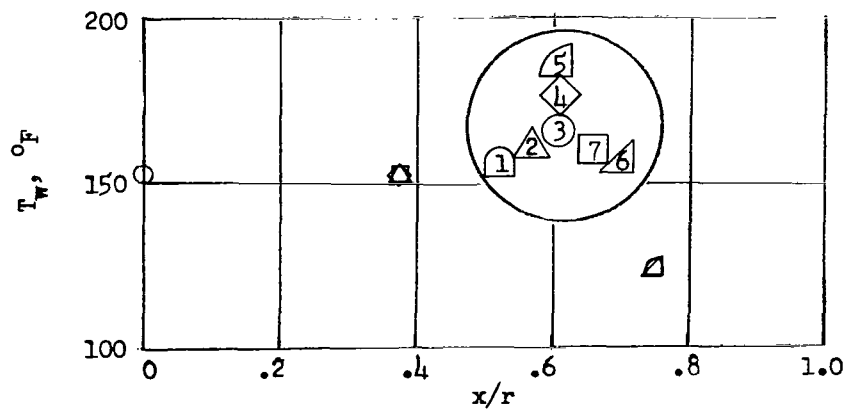
(a) 71 seconds; $M_\infty = 0.88$.
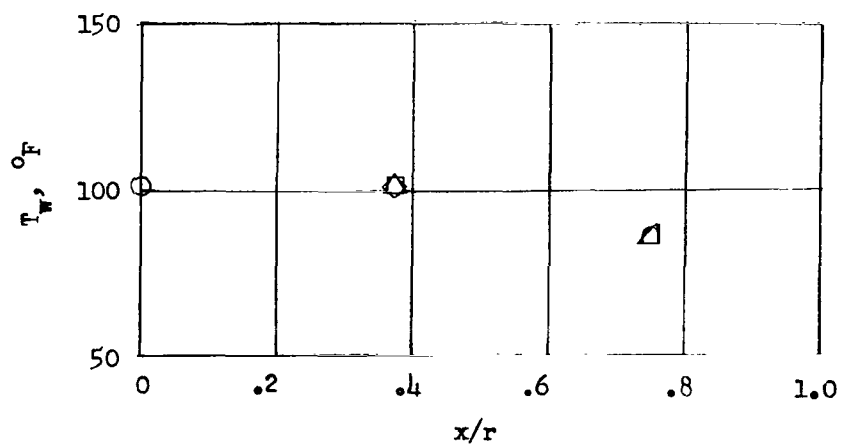
(b) 73 seconds; $M_\infty = 2.12$.
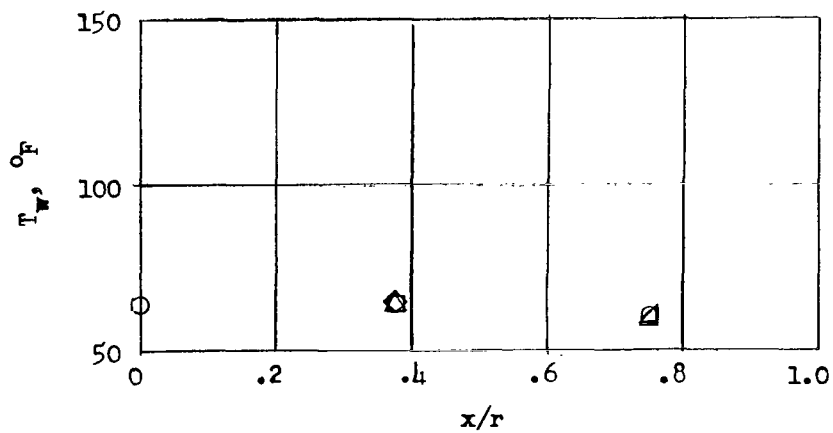
(c) 76 seconds; $M_\infty = 4.93$.

Figure 12.- Measured temperature distribution over the porous nose
for several times during flight test.
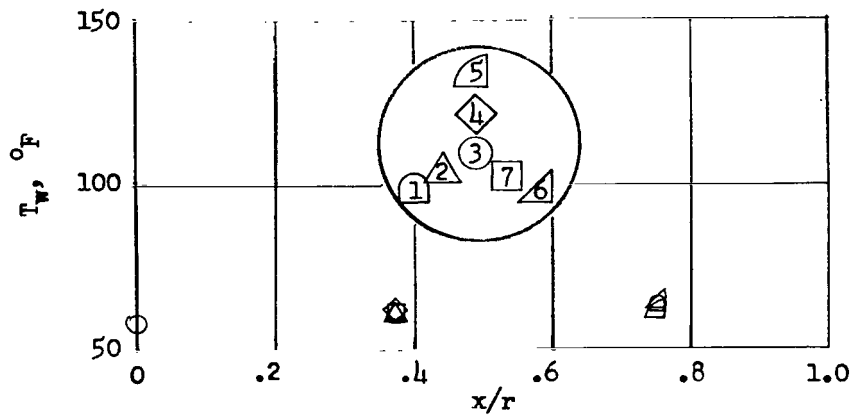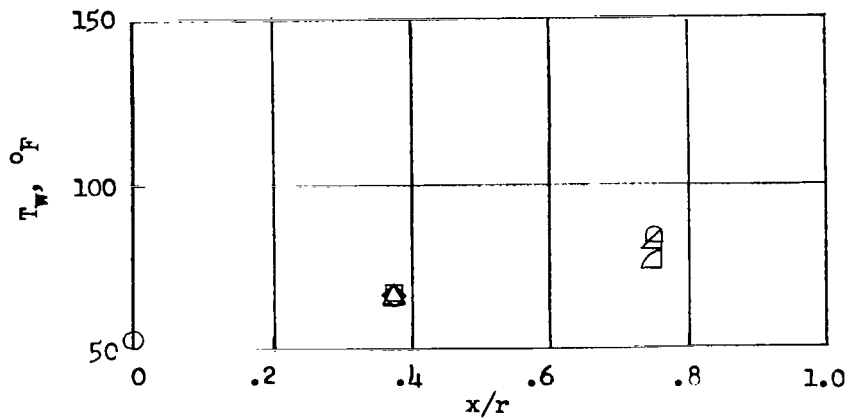
(d) 77 seconds; $M_\infty = 6.15$.
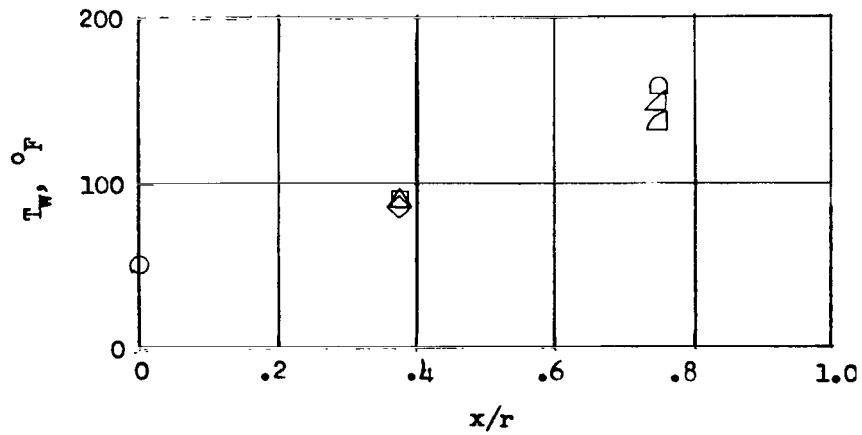
(e) 78 seconds; $M_\infty = 7.21$.

(f) 79 seconds; $M_\infty = 10.63$.

Figure 12.- Concluded.

29
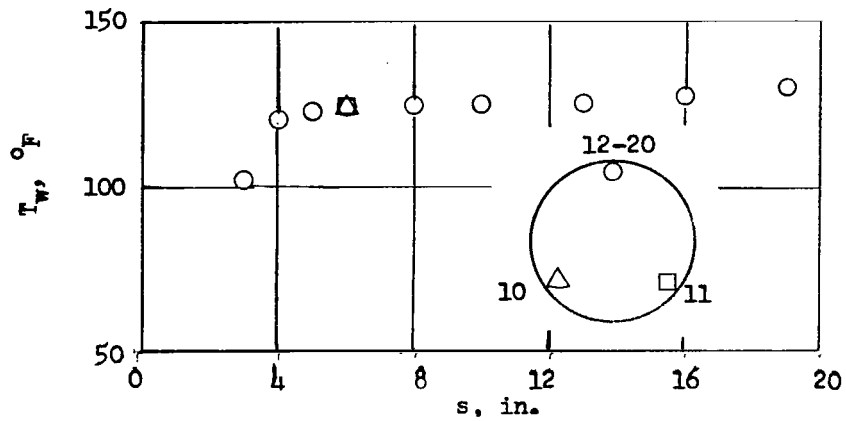
(a) 71 seconds; $M_\infty = 0.88$.
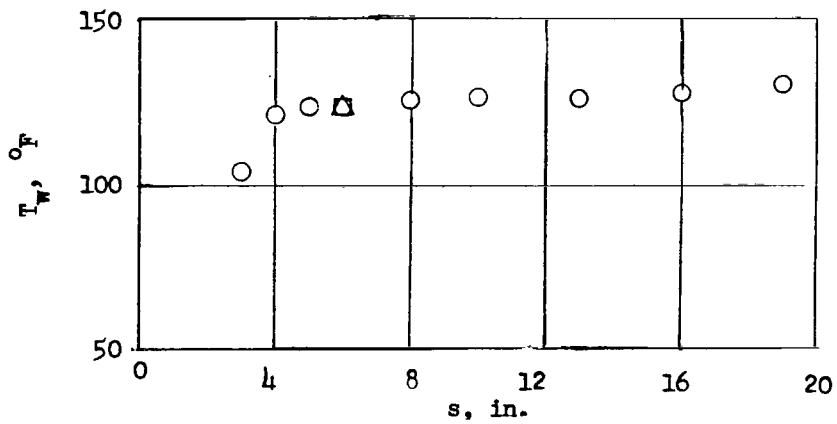
(b) 74 seconds; $M_\infty = 2.91$.
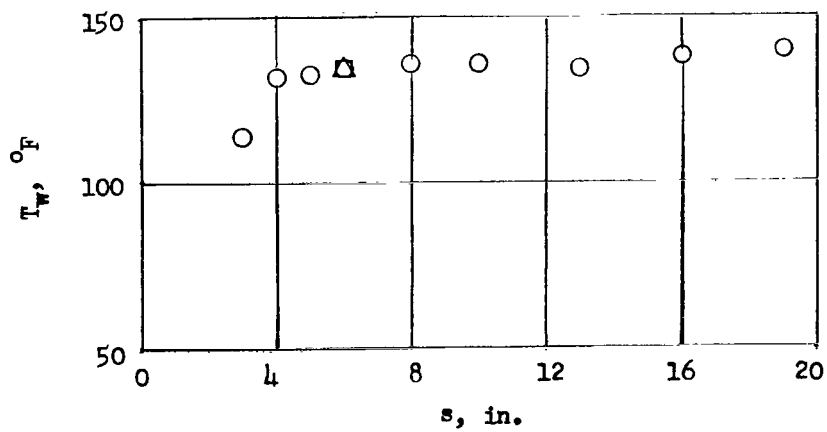
(c) 76 seconds; $M_\infty = 4.93$.

Figure 13.- Measured temperature distribution over the nonporous conical afterbody for several times during flight test.
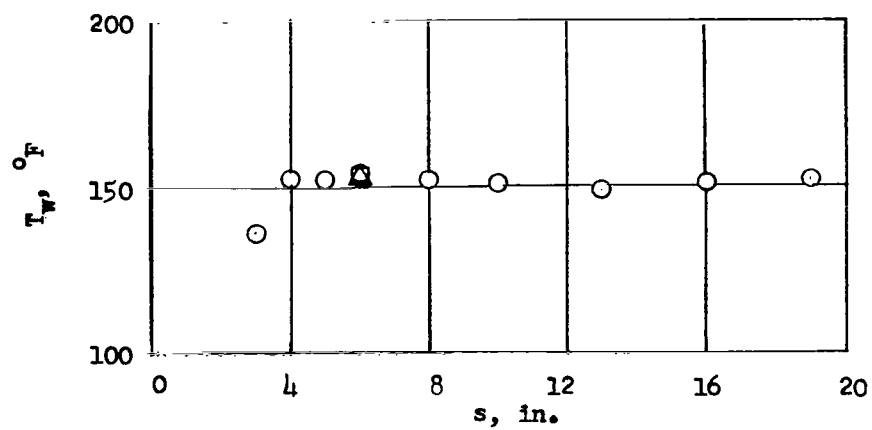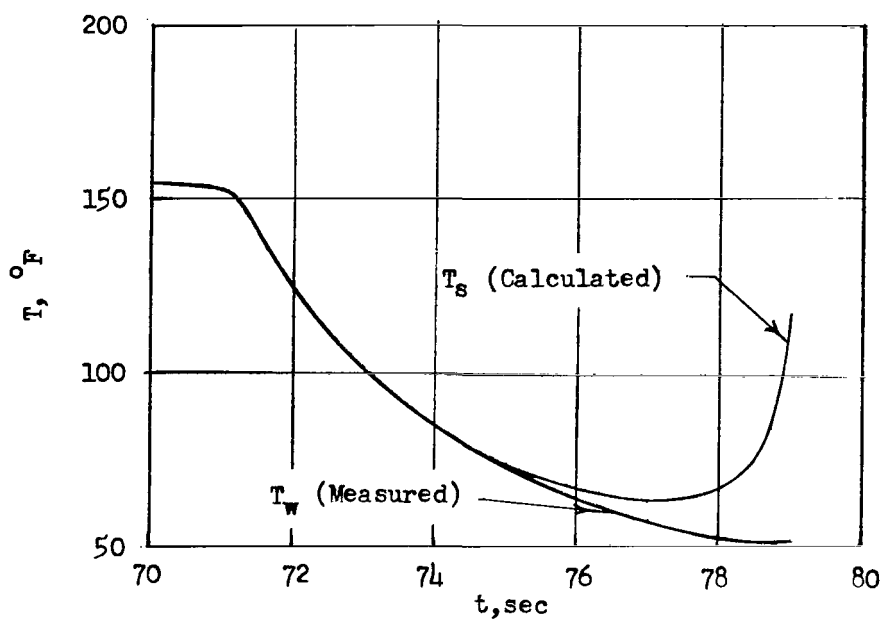
(d) 77 seconds; $M_\infty = 6.15$.
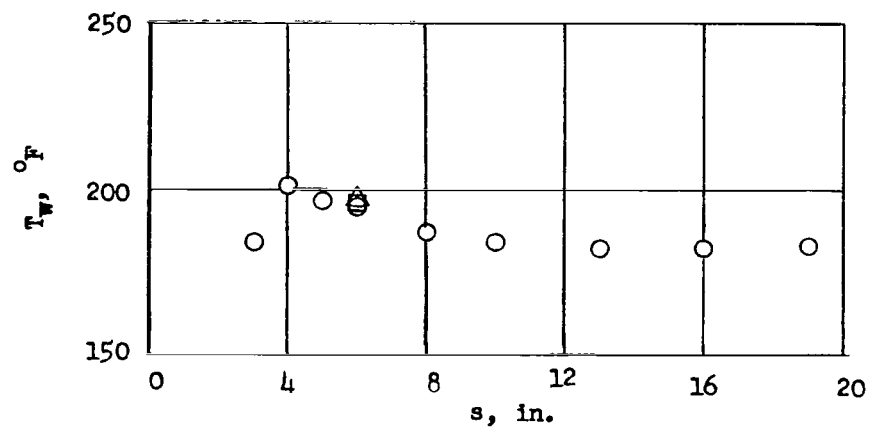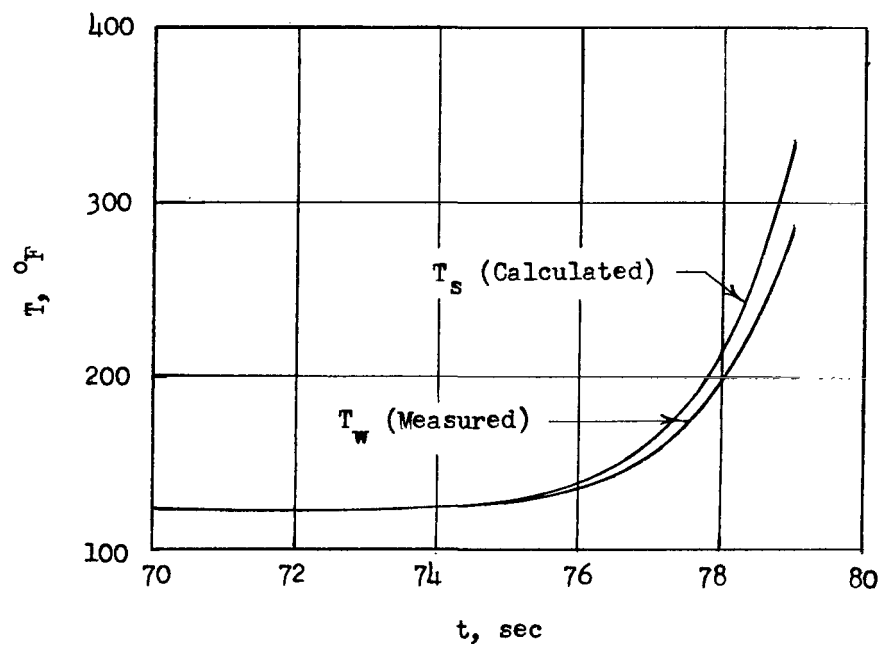

(e) 78 seconds; $M_\infty = 7.21$.
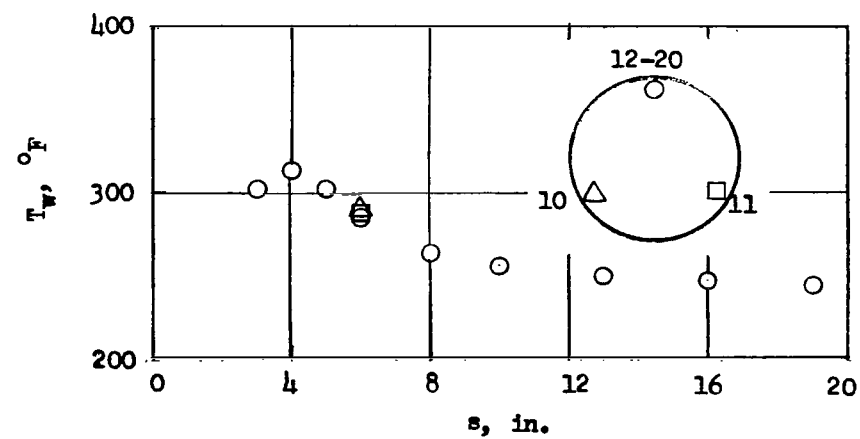
(f) 79 seconds; $M_\infty = 10.63$.

Figure 13.- Concluded.

(a) Temperature at porous nose stagnation point.

(b) Temperature at station 15 (nonporous afterbody).

Figure 14.- Time histories of typical outside and inside skin temperature on both the porous and nonporous sections of flight model.
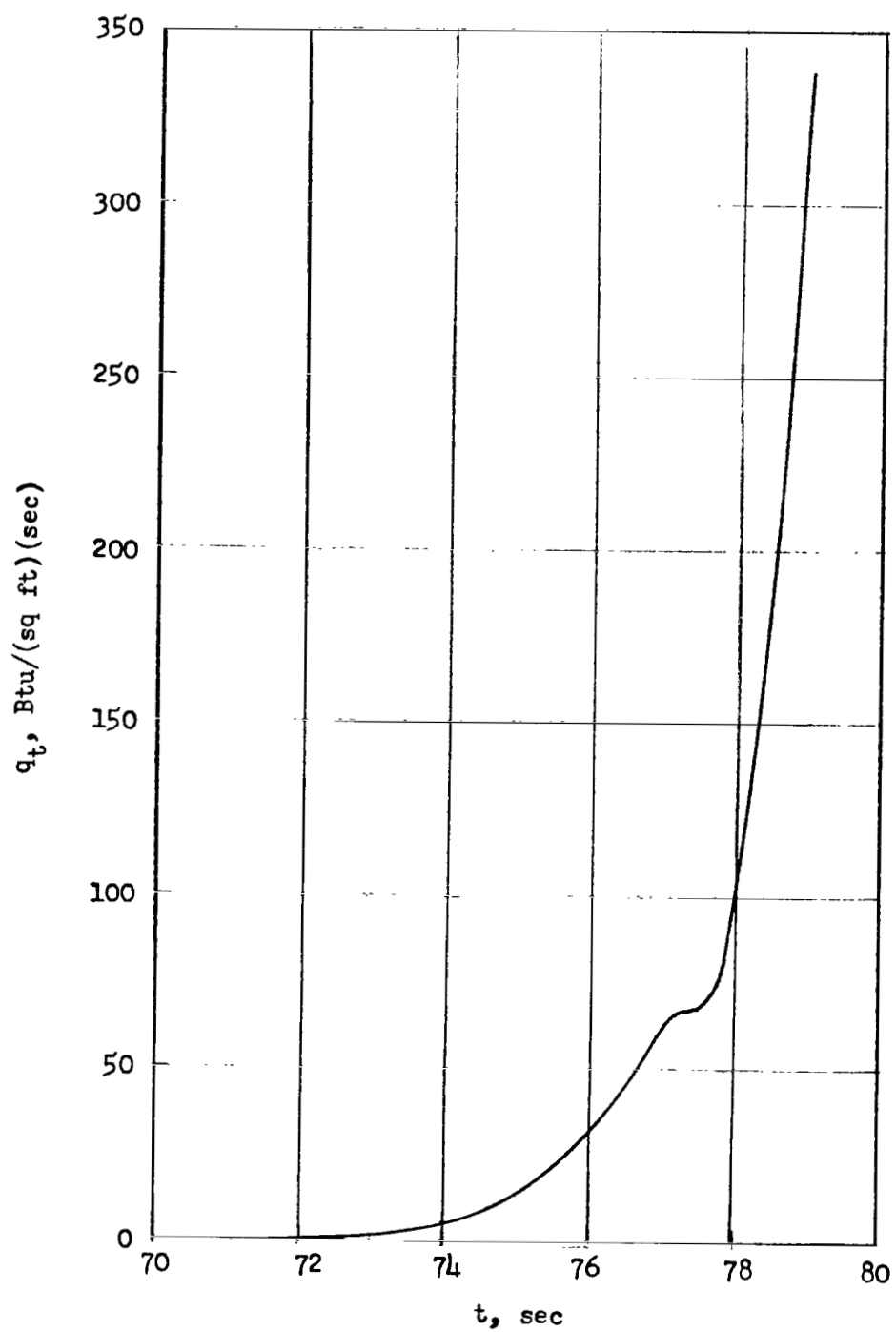
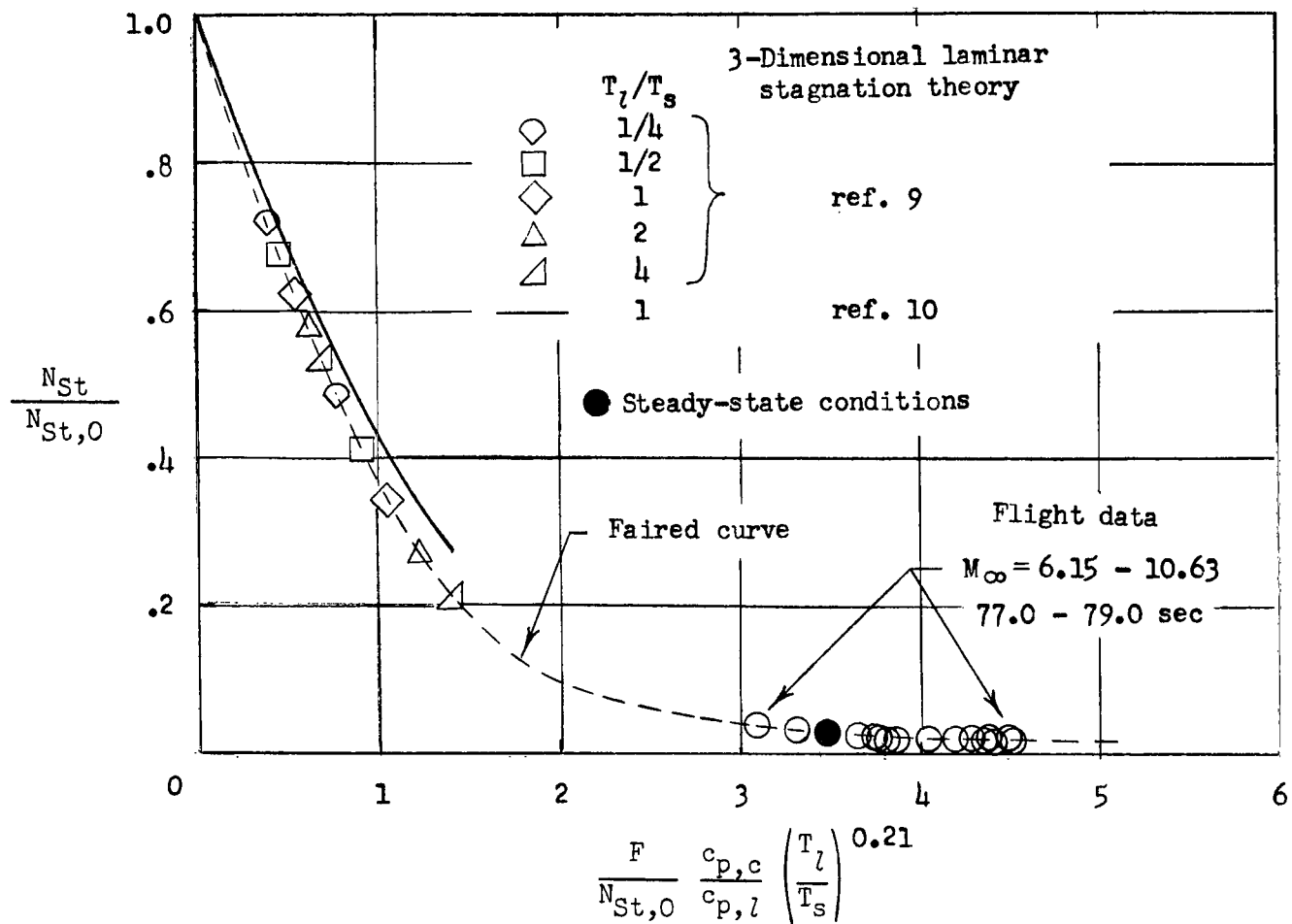Figure 15.- Theoretical stagnation-point heating rate as a function of time.

Figure 16.- Stanton number ratio as a function of flow parameter at the stagnation point of the porous nose.
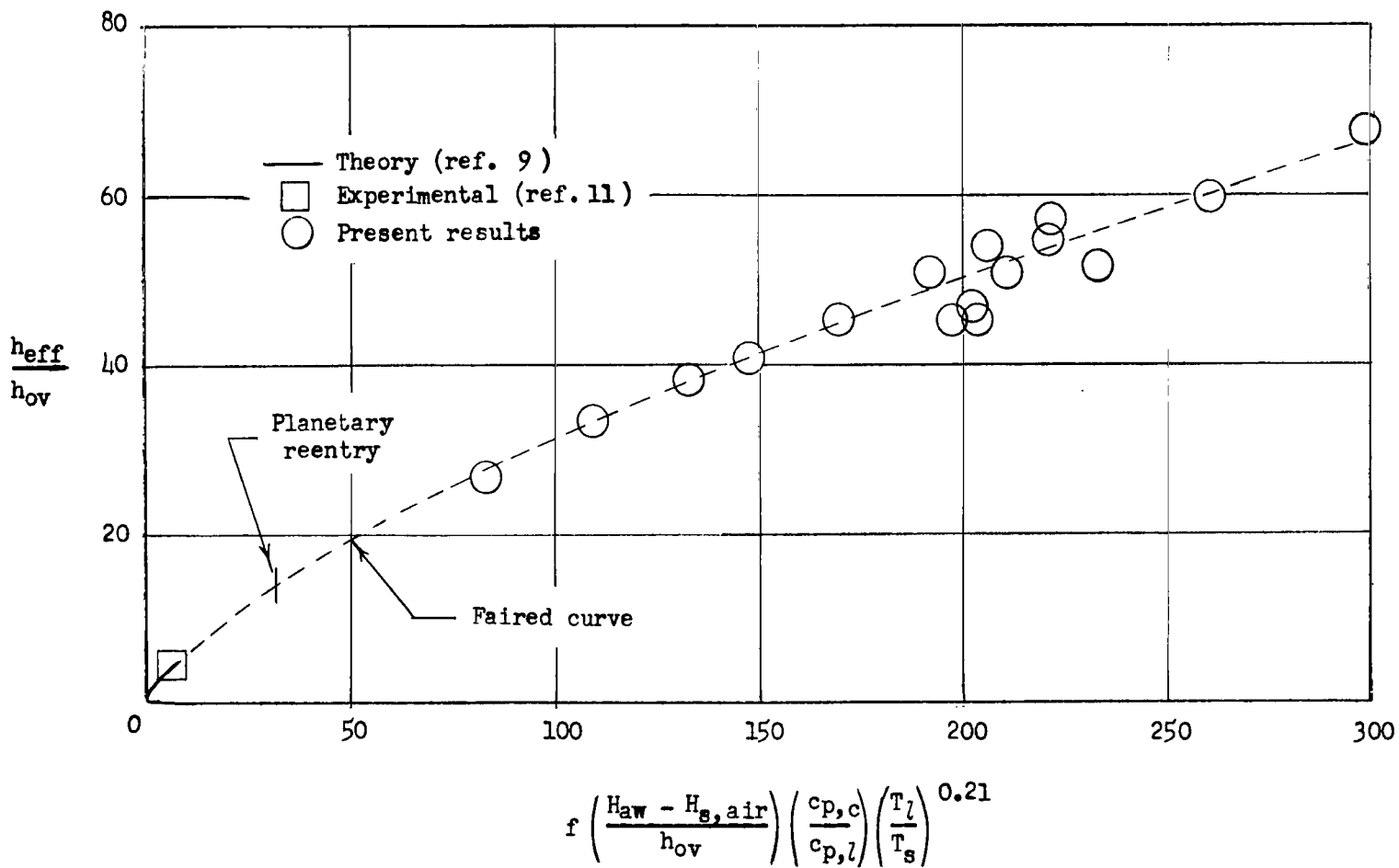
Figure 17.- Effective heat of ablation as a function of enthalpy parameter for a three-dimensional laminar stagnation boundary layer.
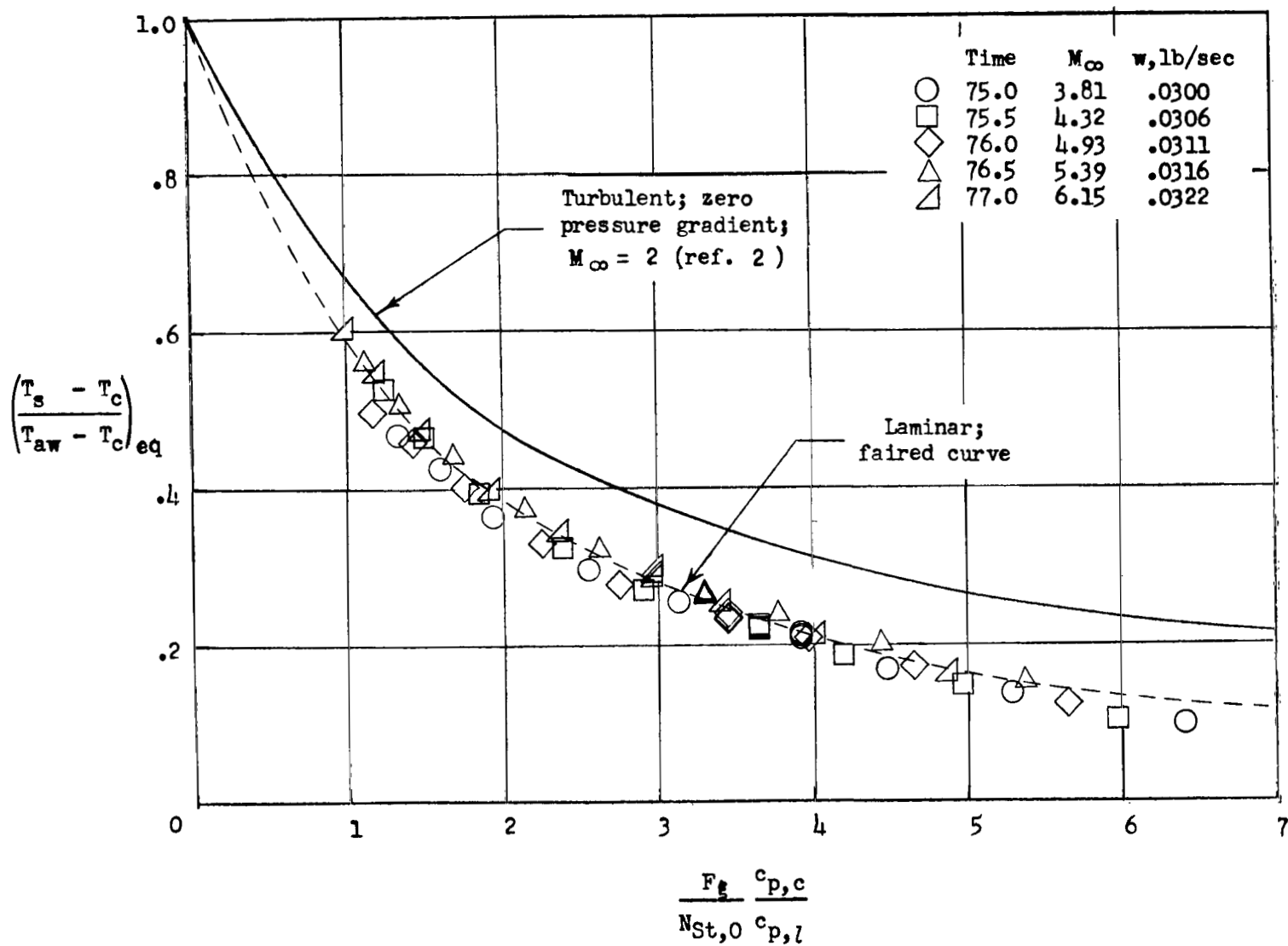
Figure 18.- Downstream cooling temperature parameter as a function of flow parameter.

"The National Aeronautics and Space Administration . . . shall . . . provide for the widest practical appropriate dissemination of information concerning its activities and the results thereof . . . objectives being the expansion of human knowledge of phenomena in the atmosphere and space."

—NATIONAL AERONAUTICS AND SPACE ACT OF 1958

NASA SCIENTIFIC AND TECHNICAL PUBLICATIONS

TECHNICAL REPORTS: Scientific and technical information considered important, complete, and a lasting contribution to existing knowledge.

TECHNICAL NOTES: Information less broad in scope but nevertheless of importance as a contribution to existing knowledge.

TECHNICAL MEMORANDUMS: Information receiving limited distribution because of preliminary data, security classification, or other reasons.

CONTRACTOR REPORTS: Technical information generated in connection with a NASA contract or grant and released under NASA auspices.

TECHNICAL TRANSLATIONS: Information published in a foreign language considered to merit NASA distribution in English.

TECHNICAL REPRINTS: Information derived from NASA activities and initially published in the form of journal articles or meeting papers.

SPECIAL PUBLICATIONS: Information derived from or of value to NASA activities but not necessarily reporting the results of individual NASA-programmed scientific efforts. Publications include conference proceedings, monographs, data compilations, handbooks, sourcebooks, and special bibliographies.

Details on the availability of these publications may be obtained from:

SCIENTIFIC AND TECHNICAL INFORMATION DIVISION

NATIONAL AERONAUTICS AND SPACE ADMINISTRATION

Washington, D.C. 20546